

Evaluation of Mg^{2+} -substituted $NiFe_2O_4$ as a green anode material

L. John Berchmans, R. Kalai Selvan, C.O. Augustin*

Central Electrochemical Research Institute, Karaikudi 630 006, India

Received 14 October 2003; accepted 15 December 2003

Abstract

In recent years, the awareness of energy, environment and economy for the metallurgical industries, has necessitated the development of mixed oxide-based oxygen-evolving anode materials to avoid the emission of greenhouse gases, such as CO_2 , CO, and CF_6 , during electrolysis. In this regard, the noncarbon anode material $Ni_{1-x}Mg_xFe_2O_4$ ($x=0.0, 0.3, 0.6, 0.9$) has been prepared by nonconventional citrate gel process using metal nitrate salts as cation precursors and citric acid as a chelating agent. The X-ray analysis showed the existence of single-phase spinel structure with increase of lattice parameter and tetrahedral radius with increasing Mg^{2+} ion concentration, as against a decrease in density. The FT-IR spectra show the characteristic features of the synthesized ferrite compounds. The DC electrical conductivity increases with increasing temperature. It also increases with an increase of Mg^{2+} ion concentration and reaches a maximum value of 3.3 S cm^{-1} at $x=0.6$ at which, the activation energy for conduction is found to be minimum. The effect of the Mg^{2+} substitution on the electrocatalytic activity of the electrodes towards the oxygen evolution reaction (OER) is studied by using steady state potentiostatic polarization measurements in alkaline KOH solution. The Roughness factor (R_f) and the Double layer capacitance (C_{dl}) of the synthesized electrodes were measured by using Electrochemical Impedance Spectroscopy. The chemical stability of the $Ni_{0.4}Mg_{0.6}Fe_2O_4$ electrode, which is observed to possess optimum properties, was ascertained in a saturated cryolite–alumina melt at the $960 \text{ }^\circ\text{C}$, the operating temperature of aluminium electrolysis.

© 2004 Elsevier B.V. All rights reserved.

Keywords: Nickel ferrite; Green anode; X-ray diffraction; Electrical conductivity; Electrochemical Impedance Spectroscopy

1. Introduction

The development of green anode materials for electro-metallurgical industries, especially for aluminium production, has gained considerable importance in recent years [1]. The significance of such anodes is their ability to produce only life-saving, environment-friendly O_2 gas during electrolysis instead of the greenhouse gases. The primary aluminium is produced by the Hall–Heroult process, by the electrodecomposition of alumina dissolved in cryolite melt maintained at $960 \text{ }^\circ\text{C}$, using the consumable carbon anodes and carbon block cathodes. During electrolysis, aluminium metal is deposited at the cathode with the liberation of CO_2 and CO at the anode. The simple electrochemical reactions taking place during

the electrolysis of alumina using green anode can be written as



Hence, the overall cell reaction may be written as



Whereas the overall cell reaction at consumable carbon anode is



The emitted CO and CO_2 cause alarming atmospheric pollution, global warming, glacier melting, rise in sea level, unpredictable climate changes, etc.

* Corresponding author. Fax: +91-4565-227713, +91-4565-227779.

E-mail address: caugustin@rediffmail.com (C.O. Augustin).

The envisaged green electrode should have high electrical conductivity, high electrocatalytic activity, thermal stability, low chemical leachability, and low overvoltage for oxygen evolution.

The mixed oxide composite materials are selected as anode materials for the above processes. Several spinel-type materials, namely, NiFe_2O_4 , NiCr_2O_4 , CoFe_2O_4 , ZnFe_2O_4 and NiAl_2O_4 [2–5], were studied as candidate anode materials for Hall cell. Nickel-based spinels are giving low chemical leachability in the saturated cryolite–alumina bath. This study has been undertaken to substitute the divalent Mg^{2+} ion for Ni^{2+} , for improving the electrical conductivity and electrocatalytic activity, and reducing chemical leachability. Among the synthetic methods, citrate gel process [6] has several potential advantages over the other methods, namely, achieving homogeneous mixing of the compounds on the atomic scale, lower processing temperature, higher purity, good control of stoichiometry, desired particle size distribution with high surface area and better sinterability. In this paper, we report the synthesis of ternary ferrite $\text{Ni}_{1-x}\text{Mg}_x\text{Fe}_2\text{O}_4$ ($x=0.0, 0.3, 0.6, 0.9$) by novel citrate gel process. The structural properties were studied by using XRD and FT-IR. The DC electrical conductivity was studied by using modified four-probe method. The electrochemical studies were made by using potentiostatic polarization and complex impedance spectroscopy. The suitability of the electrode was also studied by using weight loss method in cryolite–alumina bath.

2. Experimental

2.1. Materials synthesis

$\text{Ni}_{1-x}\text{Mg}_x\text{Fe}_2\text{O}_4$ ($x=0.0, 0.3, 0.6, 0.9$) electrodes were prepared by citrate gel process with starting materials of high-pure $\text{Ni}(\text{NO}_3)_2 \cdot 6\text{H}_2\text{O}$, $\text{Mg}(\text{NO}_3)_2 \cdot 6\text{H}_2\text{O}$, $\text{Fe}(\text{NO}_3)_3 \cdot 9\text{H}_2\text{O}$ and $\text{C}_6\text{H}_8\text{O}_7 \cdot \text{H}_2\text{O}$. The stoichiometric quantities of nitrate salts were dissolved in triple-distilled water and required amount of citric acid was added as chelating agent. Dilute aqueous ammonia was poured slowly into the nitrate–citrate mixture to adjust the pH to 6.5. The mixed solution was kept heated at 100°C for 5 h with uniform stirring and evaporated to obtain a highly viscous gel. Thus, obtained gel was placed in a hot plate and maintained at 300°C ; the gel was swelled and ignited with an evolution of large amounts of gaseous products, resulting with the desired ferrite in the form of foamy powder.

2.2. Fabrication of anodes

The $\text{Ni}_{1-x}\text{Mg}_x\text{Fe}_2\text{O}_4$ ($x=0, 0.3, 0.6, 0.9$) anodes were fabricated by high-pressure compaction followed by a sintering process. The synthesized powders were ground to obtain uniform particle size. The powders were then compacted in a hydraulic press at a pressure of 4 tons/cm^2 to

get pellets of 1 and 2.5 cm diameter with 0.5 and 3.0 cm thickness, respectively. Then, the electrodes were sintered at 1000°C in air for 50 h continuously and slowly cooled to ambient temperature.

2.3. Structural and morphological features

The crystalline phases of the prepared powders were identified by powder X-ray diffraction technique using an X-ray diffractometer $\text{Cu-K}\alpha$ radiation ($\lambda=0.1542\text{ nm}$). The FT-IR spectra of the samples were recorded as KBr discs in the range $400\text{--}1000\text{ cm}^{-1}$ by using FT-IR–Perkin Elmer, UK Paragon-500.

2.4. Electrical and electrochemical studies

The DC electrical conductivity was measured as a function of temperature of the sintered specimens using the modified four-probe method. Pt wires were used as current and potential leads, and measurements were carried out from ambient temperature to 1000°C . The resistance was measured by digital microohmmeter and the measurements were repeated for all samples with heating and cooling cycles. Temperature was measured using Cr–Al thermocouple and the temperature programmer controlled the rate of heating. Electrochemical polarization studies were performed using Volta lab-PGA201 Potentiostat/Galvanostat. Impedance measurements were carried out using PARC Electrochemical Impedance System. A conventional three-electrode system was used for the electrochemical measurements. A ‘Pt’ foil was used as the counterelectrode; a saturated Hg/HgO/1M KOH electrode was used as the reference electrode. The sintered pellet measuring 1 cm diameter and 0.5 cm thickness was used as the working electrode.

2.5. Electrode stability studies

In order to test the stability of the synthesized electrode $\text{Ni}_{0.4}\text{Mg}_{0.6}\text{Fe}_2\text{O}_4$, corrosion studies were carried out under static immersion test in saturated cryolite–alumina bath at 960°C in a graphite crucible. The samples were weighed accurately and dropped into the bath. The corrosion rate of the electrode was determined by weight loss method using the formula $r = \Delta W / \tau S$. Where r is the corrosion rate ($\text{g cm}^{-2}\text{ h}$), ΔW is the difference in weight loss (g), S is the surface area immersed with electrolyte (cm^2) and τ is the time (h).

3. Results and discussion

The X-ray powder diffraction patterns of synthesized samples $\text{Ni}_{1-x}\text{Mg}_x\text{Fe}_2\text{O}_4$ ($x=0.0, 0.3, 0.6, 0.9$) are shown in Fig. 1. It reveals that all the samples can be indexed as the single-phase cubic spinel structure. The presence of the

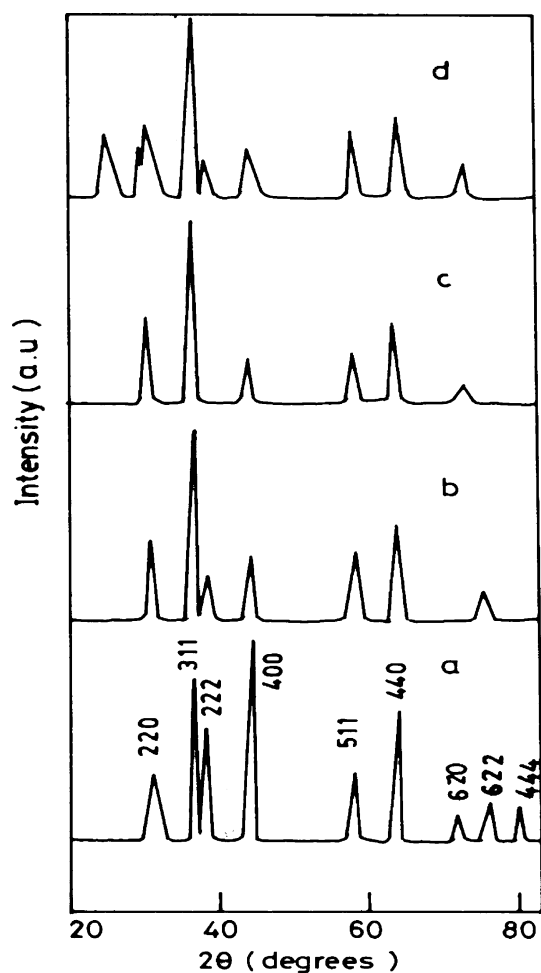


Fig. 1. XRD pattern of $\text{Ni}_{1-x}\text{Mg}_x\text{Fe}_2\text{O}_4$ (a) $x=0$, (b) $x=0.3$, (c) $x=0.6$, (d) $x=0.9$.

peaks corresponding to the planes (220), (311), (222), (400), (511), (440), (620), (622) and (444) in the pattern of the samples confirm the formation of spinel cubic structure. The intensities of the (220), (440) and (511) planes are more sensitive to the cations on tetrahedral [A site], octahedral [B site] and the oxygen ion parameters [7,8]. As reported earlier, Mg^{2+} ions have a strong preference to occupy B sites and partially occupy A sites [9] but Ni^{2+} ions occupy only B sites [10]. Table 1 shows the observed intensities of the above three planes. It can be observed that the intensity of the (440) plane decreases with the addition of Mg^{2+} ion concentration, which infers that the Ni^{2+} has preferentially occupied the B site, i.e., the octahedral site in the (440) plane. The intensity of the (220) plane is increased by the addition of Mg^{2+} ions indicating the preferential occupation of A sites up to $x=0.6$. A discrepancy is observed for $\text{Ni}_{0.1}\text{Mg}_{0.9}\text{Fe}_2\text{O}_4$ due to the structural fluctuation. The intensity of oxygen ion concentrations is decreased with the addition of Mg^{2+} concentration. The calculated lattice constant (a) values of NiFe_2O_4 ($x=0$) and $\text{Ni}_{0.1}\text{Mg}_{0.9}\text{Fe}_2\text{O}_4$ ($x=0.9$) are 0.833 nm and 0.846 nm, respectively, which are

Table 1
XRD parameters

$\text{Ni}_{1-x}\text{Mg}_x\text{Fe}_2\text{O}_4$	I_{220}	I_{440}	I_{511}	a (nm)	r_{tet} (nm)	X-ray density (g/cm^3)
$x=0.0$	43	64	44	0.833	0.640	5.380
$x=0.3$	44	47	40	0.835	0.643	5.148
$x=0.6$	48	41	35	0.836	0.646	4.909
$x=0.9$	40	38	35	0.846	0.649	4.672

well agreed with the reported values [8]. Table 1 shows the variation of lattice constant (a), tetrahedral radius (r_{tet}) and X-ray density with increase in Mg^{2+} ion concentration (x). It can be seen that there is an increase of lattice constant with Mg^{2+} ion concentration. The tetrahedral radius also increases with an increase in Mg^{2+} concentration. From the values, it can be seen that the X-ray density decreases with an increase in Mg^{2+} ion content. This may be due to the fact that the density of the Mg atom is $1.74 \text{ g}/\text{cm}^3$, which is lower than that of Ni atom, $8.91 \text{ g}/\text{cm}^3$, as well as the atomic concentration of Mg, is less ($4.3 \times 10^{22} \text{ cm}^{-3}$) compared with Ni concentration ($9.14 \times 10^{22} \text{ cm}^{-3}$) [11].

The FT-IR spectra for the $\text{Ni}_{1-x}\text{Mg}_x\text{Fe}_2\text{O}_4$ ($x=0, 0.3, 0.6, 0.9$) systems were recorded in the range $400\text{--}1000 \text{ cm}^{-1}$ and the band values are tabulated in Table 2. The spectra show two main absorption bands, ν_1 and ν_2 , corresponding to tetrahedral and octahedral sites around 600 and 400 cm^{-1} , respectively. The spectra for pure NiFe_2O_4 show the splitting of absorption bands. The band ν_2^* at 419.66 cm^{-1} has a subsidiary band ν_2' at 471.87 cm^{-1} . This subsidiary may be due to the Jahn–Teller distortion produced by Fe^{2+} ions which produce local deformation in the crystal field potential and hence, splitting of the absorption band [12]. The spectra also show a change in shift due to the introduction of Mg^{2+} ions. The tetrahedral site bands are shifted from higher band values to lower band values, i.e., $613.54\text{--}585.41 \text{ cm}^{-1}$, which can be attributed to the shifting of Fe^{3+} ions towards oxygen ion on occupation of tetrahedral site by Mg^{2+} ions with larger ionic radii which decreases the $\text{Fe}^{3+}\text{--O}^{2-}$ distance [13]. The octahedral site bands are shifted from lower to higher values, i.e., $419.66\text{--}434.74 \text{ cm}^{-1}$. The observed values illustrate that the frequency bands, which appeared at 417 and 604 cm^{-1} , are responsible for the formation of NiFe_2O_4 [14].

Table 2
FT-IR parameters

Sites	Band (cm^{-1})	$x=0.0$	$x=0.3$	$x=0.6$	$x=0.9$	Me--O^{2-}
A	γ_1^*	613	601	591	585	$\text{Fe}^{3+}\text{--O}^{2-}$
B	γ_2^*	419	429	432	434	Ni–O
	γ_{sh}	471				
γ_{th}		450	460	470	485	
E_{th} (eV)		0.056	0.057	0.058	0.060	

Table 3
DC electrical parameters

Electrodes	σ at 1000 °C (S cm ⁻¹)	E_{σ} (eV)
NiFe ₂ O ₄	1.90	0.3279
Ni _{0.7} Mg _{0.3} Fe ₂ O ₄	2.53	0.2589
Ni _{0.4} Mg _{0.6} Fe ₂ O ₄	3.30	0.1918
Ni _{0.1} Mg _{0.9} Fe ₂ O ₄	0.43	0.6903

The DC electrical conductivity of the electrodes increases with the increase in temperature. Increase in Mg²⁺ ion concentration also enhances the conductivity up to $x=0.6$. The conducting mechanism of nickel ferrite can be explained by the following redox reactions.



Combining these two equations,



Nickel ferrite has an inverse spinel structure and the cation distribution is as follows: (Fe³⁺)_A [Ni²⁺Fe³⁺]_B O₄. As the concentration of Mg²⁺ ion in the synthesized material increases, some of the Mg²⁺ ions may occupy tetrahedral sites, resulting a migration of Fe³⁺ ions into octahedral sites. The increase in concentration of Fe³⁺ ions at B sites increases the hopping rate of electrons, which in turn enhances the conductivity to maximum (3.3 S cm⁻¹ at $x=0.6$). In contrast, the lower specific conductivity of 0.8 S cm⁻¹ obtained for the specimen Ni_{0.1}Mg_{0.9}Fe₂O₄ may be due to the meager amounts of ferrous and ferric ions at B sites.

Table 3 represents the variation of activation energy and specific conductivity measured at 1000 °C with Mg²⁺ ion concentration. From the table, it is observed that the activation energy decreases with the increase in concentration of Mg²⁺ ions up to $x=0.6$, whereas in the case of $x=0.9$, the activation energy is maximum, causing a lower conductivity. In Ni_{0.4}Mg_{0.6}Fe₂O₄, the activation energy is found to be lowest because of the energy required for electron hopping between Fe²⁺ and Fe³⁺ is rather low, leading to high conduction.

4. Electrochemical studies

The IR-compensated steady state polarization curve for oxygen evolution on a Ni_{1-x}Mg_xFe₂O₄ ($x=0.0, 0.3, 0.6, 0.9$) electrodes at 1 M KOH solution are shown in Fig. 2. The electrode kinetic parameter for the oxygen evolution reaction (OER), i.e., oxygen overpotential (η_{O_2}) at 1.5 mA/cm², Tafel slope at lower and higher overpotentials are summarized in Table 4. Based on the oxygen overpotential at a fixed current density of 1.5 mA/cm², the electrodes

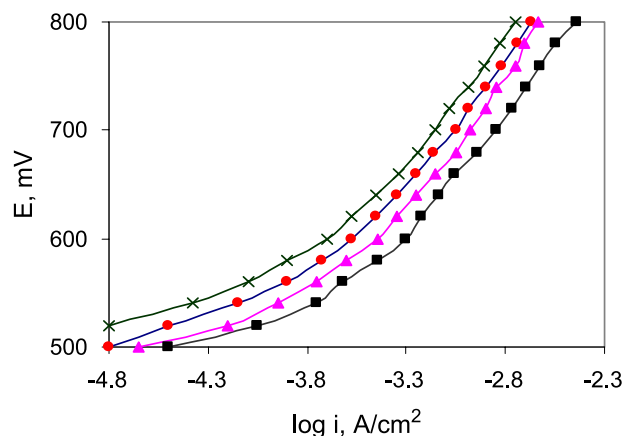
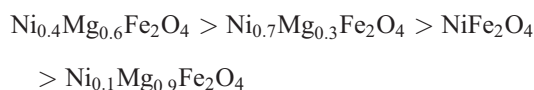


Fig. 2. The Tafel plot of Ni_{1-x}Mg_xFe₂O₄ (●) $x=0$, (▲) $x=0.3$, (■) $x=0.6$, (x) $x=0.9$.

graded in the decreasing order of electrocatalytic activity is as follows.

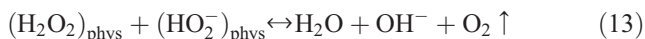
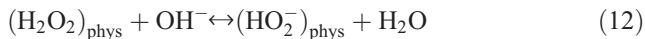


The oxygen overpotential for Ni_{0.4}Mg_{0.6}Fe₂O₄ was very low compared with other electrodes. This may be due to the substitution of Mg²⁺ ions, which creates the change in reaction mechanism, and consequently, the intrinsic activity of the base material [15]. It is seen that the Tafel slopes in the lower and higher potential regions are 50–90 and 200–230 mV/dec, respectively, which are in agreement with the value reported on NiFe₂O₄, prepared by thermal decomposition method using metal nitrate salts at 1150 °C [16]. When the Mg²⁺ ions are incorporated into the parent compound, the Tafel slope increases both lower and higher overpotential regions up to Ni_{0.4}Mg_{0.6}Fe₂O₄. At the lower overpotential region, the Tafel slope may be due to the oxygen evolution on activation-controlled process, whereas at the high potential region, it may be due to the change in rate-determining step [17]. In spinel-type oxides, the B site active cations are directly linked with the catalytic activity and Tafel slope. As discussed earlier, the replacement of Ni²⁺ ions from octahedral sites and the presence of active cations Fe²⁺/Fe³⁺, Ni²⁺/Ni³⁺ and Mg⁺/Mg²⁺ are increased in the B site, enhancing the overall catalytic activity which is confirmed from the XRD and electrical conductivity

Table 4
Electrode kinetic parameters for oxygen evolution

Electrodes	η_{O_2} at 1.5 mA/cm ² (mV)	Tafel slope	
		Low η (mV/dec)	High η (mV/dec)
NiFe ₂ O ₄	457	80	214
Ni _{0.7} Mg _{0.3} Fe ₂ O ₄	437	80	226
Ni _{0.4} Mg _{0.6} Fe ₂ O ₄	402	90	228
Ni _{0.1} Mg _{0.9} Fe ₂ O ₄	482	52	204

measurements [18]. The reaction mechanism of the oxygen evolution of the synthesized electrode is as follows [19].



Where, M^z is a transition metal ion with a valency state z^+ at the surface of the spinel.

The complex impedance Bode plots for the synthesized electrode $Ni_{1-x}Mg_xFe_2O_4$ ($x=0.0, 0.3, 0.6, 0.9$) in 1 M KOH are shown in Fig. 3. The high-frequency plot has been associated with the charge transfer process and the low-frequency plot with the mass transfer process. The electrochemically active area, i.e., the Roughness factor (R_f), of the electrocatalyst was estimated from the ratio of double-layer capacitance (C_{dl}) and the C_{dl} of the smooth oxide surface ($60 \mu\text{F}/\text{cm}^2$). The C_{dl} of the synthesized $Ni_{1-x}Mg_xFe_2O_4$ ($x=0.0, 0.3, 0.6, 0.9$) electrode was estimated by extrapolating the linear capacitance region to the $\log|Z|$ axis at $\omega=1$ or $f=0.16$ Hz as described elsewhere [20]. The R_f and C_{dl} values of the synthesized samples are given in Table 5. From the table, it can be observed that as the substitution of Mg^{2+} ion concentration increases, the roughness factor and the

Table 5

AC impedance parameters

Electrodes	$ Z $ (Ω)	C_{dl} (mF/cm^2)	R_f	$-\theta$
$NiFe_2O_4$	151.9	6.583	109.7	48.0
$Ni_{0.7}Mg_{0.3}Fe_2O_4$	240.9	4.151	069.1	62.5
$Ni_{0.4}Mg_{0.6}Fe_2O_4$	401.8	2.480	041.3	56.0
$Ni_{0.1}Mg_{0.9}Fe_2O_4$	974.2	1.026	017.1	50.0

double-layer capacitance decreases. It can be inferred that as the C_{dl} value decreases, the degradation of the material decreases. Hence, it can be concluded that the synthesized electrode material with maximum Mg^{2+} ion concentration is more stable in the corrosive environments.

4.1. Chemical stability

To determine the stability of the electrode, the weight loss method is more effective compared with other corrosion-monitoring methods. The corrosion rate of the synthesized $Ni_{0.4}Mg_{0.6}Fe_2O_4$ electrode is $0.035 \text{ g}/\text{cm}^2 \text{ h}$. The higher value may be due to the lower density and lower sintering temperature. Due to the lower density, the intergranular corrosion is dominated via the disintegration, grain boundary attack and chemical dissolution [21]. The corrosion rate of the electrode will hopefully be decreased by increasing the sintering temperature up to 1500°C .

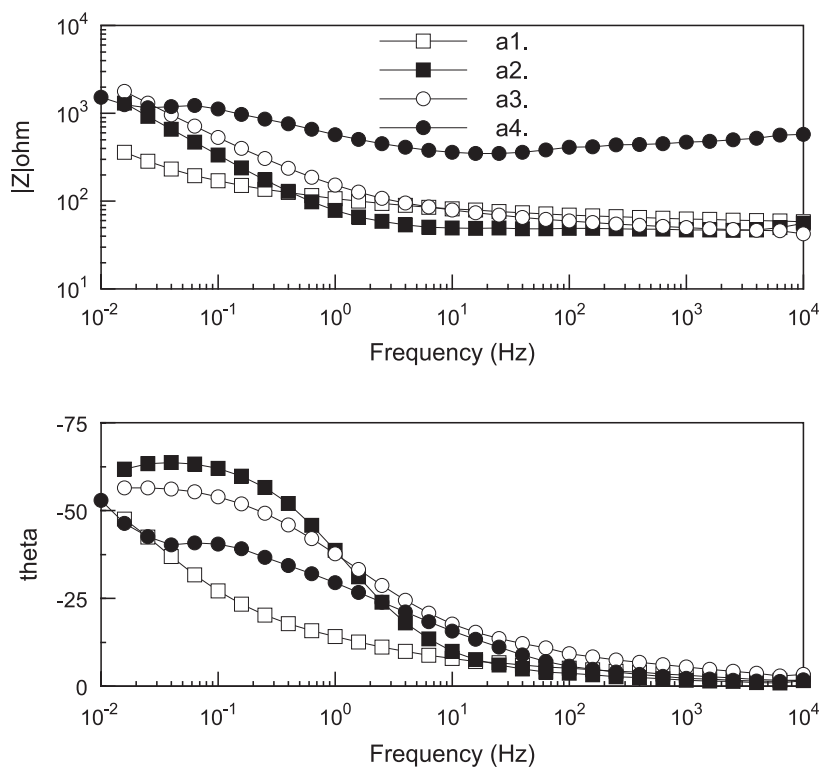


Fig. 3. Complex impedance Bode plot of $Ni_{1-x}Mg_xFe_2O_4$ (a1) $x=0$, (a2) $x=0.3$, (a3) $x=0.6$, (a4) $x=0.9$.

5. Conclusions

The Citrate-gel process is found to be a simple and effective method for the preparation of electrode materials. The XRD pattern shows that the synthesized materials are in cubic structure. The electrical conductivity for $\text{Ni}_{0.4}\text{Mg}_{0.6}\text{Fe}_2\text{O}_4$ is 3.3 S cm^{-1} , which is comparatively maximum, and the electrochemical studies of the above material show higher catalytic activity and stability in corrosive environments. The weight loss method also confirms the suitability of the Mg^{2+} -substituted ($x=0.6$) electrode in cryolite–alumina bath. Hence, it may be concluded, that, by the substitution of Mg^{2+} ion in the NiFe_2O_4 , the overall electrical conductivity, sinterability, electrocatalytic activity, thermal and chemical stability have been found to increase, making the $\text{Ni}_{0.4}\text{Mg}_{0.6}\text{Fe}_2\text{O}_4$, the more suitable green anode for electrometallurgical industries.

Acknowledgements

The authors express their gratitude to the Director, CECRI, and to the staff of the Electropyrometallurgy Division and Characterization laboratory for their kind help.

References

- [1] L. John Berchmans, C.O. Augustin and, U. Sen, *Minerals & Metals Review* XXVI (2000) 55.
- [2] E. Olsen, J. Thonstad, *Journal of Applied Chemistry* 29 (1999) 301.
- [3] C.O. Augustin, D. Prabhakaran, L.K. Srinivasan, *Journal of Materials Science Letters* 12 (1993) 383.
- [4] R.P. Pawlek, *Light Metal Age* 60 (2002) 50.
- [5] T.E. Jentoftsen, O.A. Loventsen, G.M. Hearberg, J. Thonstad, *Metallurgical and Materials Transactions. B, Process Metallurgy and Materials Processing Science* 33B (2002) 901.
- [6] A. Prasad, N.S. Gajbhiye, *Journal of Alloys and Compounds* 265 (1998) 87.
- [7] B.P. Ladgaonkar, A.S. Vaingainkar, *Materials Chemistry and Physics* 56 (1998) 280.
- [8] C.S. Narasimhan, C.S. Swamy, *Physical Status Solidi (a)* 59 (1980) 817.
- [9] R. Kulkarni, H. Joshi, *Solid State Communications* 53 (1985) 1005.
- [10] B.V. Bhise, M.B. Dongar, S.A. Patil, S.R. Sawant, *Journal of Materials Science Letters* 10 (1991) 922.
- [11] C. Kittel, *Introduction to Solid State Physics*, 7th Ed., Wiley, New York, 1996, p. 24.
- [12] V.A. Potakova, N.D. Zveru, V.P. Romanov, *Physical Status Solidi (a)* 12 (1972) 623.
- [13] S.C. Watawe, B.D. Sutov, B.D. Sarwade, B.K. Chougale, *International Journal of Inorganic Materials* 3 (2001) 819.
- [14] S. Music, D. Balzar, M. Gotic, S. Popovic, S. Dalipi, *Croatica Chemica Acta* 70 (1997) 719.
- [15] M.H. Mendonca, M.I. Godiho, M.A. Catarino, F.M. Costa, *Solid State Sciences* 4 (2000) 175.
- [16] N.K. Singh, R.N. Singh, *Indian Journal of Chemistry* 38A (1999) 491.
- [17] F. Svegl, B. Orel, I.G. Svegl, V. Kaucic, *Electrochimica Acta* 45 (2000) 4359.
- [18] R.N. Singh, N.K. Singh, J.P. Singh, *Electrochimica Acta* 47 (2002) 3873.
- [19] L. Formaro and, M. Longhi, *Journal of Physical Chemistry B* 107 (2003) 6425.
- [20] R.N. Singh, B. Lal, *International Journal of Hydrogen Energy* 27 (2002) 45.
- [21] H. Xiao, R. Herland, S. Rolseth, J. Thonstad, *Metallurgical and Materials Transactions. B, Process Metallurgy and Materials Processing Science* 27B (1996) 185.